A phenomenological model of cell-cell adhesion mediated by cadherins

Simona Mancini, René-Marc Mège, Benoit Sarels, Pierre-Olivier Strale

Noname manuscript No.
(will be inserted by the editor)

A phenomenological model of cell-cell adhesion mediated by cadherins

Simona Mancini · René-Marc Mège · Benoit Sarels · Pierre-Oliveir Strale

Received: date / Accepted: date

Abstract We present a phenomenological model intended to describe at the protein population level the formation of cell-cell junctions by the local recruitment of homophilic cadherin adhesion receptors. This modeling may have a much wider implication in biological processes since many adhesion receptors, channel proteins and other membrane-born proteins associate in clusters or oligomers at the cell surface. Mathematically, it consists in a degenerate reaction-diffusion system of two partial differential equations, modeling the time-space evolution of two cadherin populations over a substrate : the first one representing the diffusing cadherins and the second one concerning the fixed ones. After discussing the stability of the solutions of the model, we perform numerical simulations and show relevant analogies with experimental results. In particular, we show patterns or aggregate formation for a certain set of parameters. Thus, perturbing the stationary solution, both density populations converges in large times to some saturation level. Also the exponential rate of convergence is numerically obtained and is shown to be in agreement, for a suitable set of parameter, with the one obtained in some in vitro experiments.

S. Mancini
Laboratoire MAPMO, UMR 7349, Fédération D. Poisson, BP. 6759, Université of Orléans, 45067 Orléans, France

Laboratoire TIMC-IMAG, Faculté de Médecine de Grenoble, 38706 La Tronche, France
Tel.: +33-4-56520045 Fax: +33-4-56050022 E-mail: simona.mancini@math.cnrs.fr

· R.-M. Mège · P.-O. Strale
Institut Jacques Monod, Centre National de la Recherche Scientifique, Université Paris Diderot, 75205 Paris, France

B. Sarels
Sorbonne Universités, UPMC Université Paris 06, CNRS, Laboratoire JLL, 4 place Jussieu 75005 Paris,
Laboratoire BI2M, place Georges Teissier 29680 Roscoff, France

Keywords Cell Adhesion · Cadherins · Adherens Junctions · Protein Clustering · Degenrate Reaction-Diffusion System · Patterns Formation

Mathematics Subject Classification (2000) MSC 92C15 · MSC 82B21 · MSC 35J70

1 Introduction

Intercellular junctions are macromolecular structures, built at the interface between cell membranes, that hold animal cells together within a tissue. Two of these types of junctions, *adherens* junctions and desmosomes are formed by the local recruitment of transmembrane proteins of the cadherin family tightly associated intracellularly to the cytoskeleton which provides cells with particular viscoelastic properties and mechanical resistance. *Adherens* junctions are of particular importance because their initiate the formation of all the other types of intercellular junctions, including desmosomes, and thus are at the centre of the cohesion and mechanical resistance of tissues of multicellular organisms. So *adherens* junction formation deserved much interest among experimental biologists. Cell-cell adhesion associated to adherens junction formation is initiated by the homophilic trans-interaction of extracellular domain of cadherins from two adjacent cells [7]. The strengthening of adhesion is then favored by the clustering of cadherin molecules in the two membranes and by the anchoring of their cytoplasmic domain, via catenin adapter protein, to the underlying actin filaments (F-actin), themselves maintained under tension by non-muscle myosin motors (myosin II). However, the sequence of molecular and cellular events leading to the formation of mature *adherens* junctions from this initial cell-cell adhesion event is still unclear, likely because of the high variability of cell-cell contact shapes and because of the multitude of partners and regulatory steps involved. In particular, how the trans-interaction of cadherin ectodomains leads to the clustering and anchoring to F-actin of cadherin adhesion complexes to form discrete size-defined junctional areas [7,4,3]. To overcome these difficulties we described earlier an experimental approach where single cells are allowed to spread on surfaces covered with cadherin extracellular domains, mimicking cell-cell contact formation [2]. On such a substratum, cells adopt a flat morphology with radial accumulations of cadherin adhesion complexes on their ventral face that colocalize with F-actin mimicking the formation of *adherens* junctions (Fig. 1).

Interestingly, these local accumulations of cadherins were also formed when the F-actin network was destructured by pharmacological means, indicating that cadherin clusters formation could be dictated by trans-interactions of cadherin ectodomains, [6]. However, how solely such interactions could generated the observed patterned distribution of cadherins is not obvious. Interestingly, cadherin dense regions correspond to areas of strong membrane apposition to the adhesive surface, [6]. In between cadherin accumulations, membrane is significantly remote from the substratum, likely as a result of either the repulsion

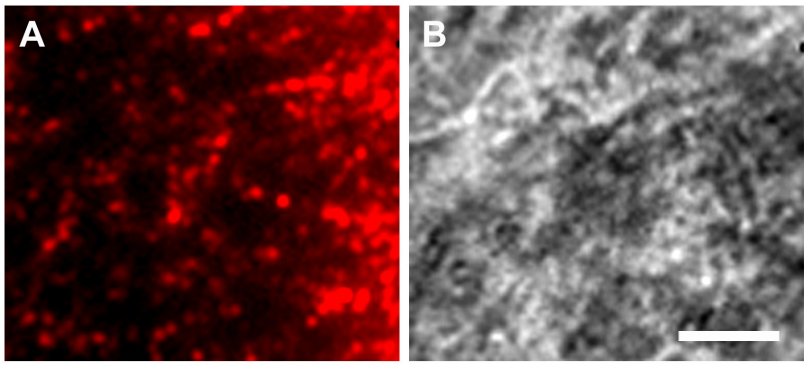

Fig. 1 (A): example of accumulation of immunofluorescently labelled cadherin adhesion complexes in cells seeded on a glass coverslip coated at saturation with recombinant cadherin ectodomain. The signal is detected by total internal reflection fluorescence microscopy (TIRFM); the brightest is the signal, the stronger is the local accumulation of cadherins. Notice the accumulation in hot spots. (B) : Reflection interference contrast microscopy (RICM) imaging of the same cell region objectivizing the distance separating locally the cell membrane from the glass coverslip. The closest the membrane is from the membrane, the darker is the signal. Scale bar: 5 μm. Notice the preferential accumulation of cadherins in areas of lowest membrane distance. The aligned hot spots at the cell periphery are associated to radial actin cables pushing the membrane close to the substratum. Extracted from [6].

exerted by larger extracellular glycoproteins or of spontaneously occurring active plasma membrane fluctuation, [1,11].

In the present study, we propose a mathematical model describing the contribution of cadherin trans interactions to their local recruitment in adhesion plaques neglecting the interaction with the actin filaments. The model takes into account the diffusive properties of cadherins and their binding and unbinding probabilities. It is a macroscopic model describing the time and space evolution of two densities distribution functions, one for the freely diffusing cadherins and one for the fixed ones. Since one of the two population of cadherins does not diffuse and since the two populations interact, the system of partial differential equations we will consider is a degenerate reaction-diffusion system. It will be numerically shown that the solution of the system is strongly dependent on the initial density distribution, and we shall therefore validate our model comparing, rather than the distribution of aggregates, the time evolution of the proportion of free and linked cadherins with those obtained by experiments.

The paper is organized as follows. In Sect. 2 we resume the basic biological features and define the mathematical model. Its mathematical analysis is performed in Sect. 3 : after proving that the stationary solution of the considered system are homogeneous in space, we perform a stability analysis to prove that taking the parameters in some range leads to structure formations.

Sect. 4 is devoted to the numerical approach : first we show the behavior of the solution on some theoretical tests, then we consider more biological tests and compare the numerical results with experimental ones. Some discussions are finally given in Sect. 5.

2 The mathematical model

We aim at modeling the clustering of cadherins seen at the mesoscopic scale on cells spread on cadherin-coated surfaces (see Fig. 1). This problem is thus bi-dimensional and we consider a bounded domain $\Omega \subset \mathbb{R}^2$. In a first approximation, we simplify the problem making the following assumptions :

- On the substrate, there is a coating of cadherins that mimics the surface of a neighboring cell. We shall call these cadherins the *targets* and we assume that their number is constant in time and that they are uniformly distributed on the domain Ω. We describe them in the mathematical model by their density $\rho > 0$. Note that these targets are fixed, hence they do not diffuse.
- Over the substrate is the cell membrane on which cadherins diffuse and bind to the substrate. The distance between the substrate and the membrane being negligible, we may say that the considered cadherins evolve on the substrate itself. We consider two populations of cadherins : those diffusing, whose density distribution will be denoted by $u = u(x,t)$ and which we refer to as *free cadherins* ; and those linked to the substrate, whose density distribution will be denoted by $v(x,t)$ and which we will call *fixed cadherins*.
- The cadherins are able to bind to form trans- bounds. The probability for a diffusing cadherin to bound is locally increased by the presence of other fixed cadherins, see [1,11]. This will be represented by a non-linear increasing, positive and bounded function $F(v)$, which we will refer to as the *aggregation function*.
- Fixed cadherins may unbind. The probability of a fixed cadherin to unbind locally depends on the presence of other fixed cadherins, the more of bounds are present the harder the cadherin unbind. This will be given by a non-linear decreasing, positive and bounded function $G(v)$, denoted also as the *unbinding function*.
- As it is shown in [5] following their trajectories, cadherins which aren't linked to some actin filament diffuse and, once they get linked to some filament, their trajectory becomes straighter, the diffusion coefficient loosing two order of magnitude. We then assume that free cadherins diffuse on the membrane while fixed cadherins do not. This is justified also by the experimental framework in which cadherins bind on fixed targets which mimic the other cell membrane.

The mathematical model describing the biological phenomena we consider is thus described at a macroscopic level by the following degenerate reaction-

diffusion system,

$$\begin{cases} \partial_t u = \sigma \, \Delta u - \varepsilon r(u, v) \\ \partial_t v = \varepsilon r(u, v) \end{cases} \tag{1}$$

where σ is the diffusion coefficient and ε is a parameter describing the efficacy of the reaction term on the evolution in terms of a frequency. System (1) is composed of a reaction-diffusion equation and a reaction equation (a simple time evolution partial differential equation) respectively on the unknown density functions $u = u(x, t)$ and $v = v(x, t)$, which represent the distributions of free and fixed cadherins at time $t \geq 0$ and in a position $x \in \Omega$. Since $\Omega \subset \mathbb{R}^2$, x is a two-component vector and Δ is the Laplacian operator with respect to the two components of x. Note that u and v being two densities, they must be non-negative at all time. Moreover, from a biological point of view, it is not possible to have more fixed cadherins than the possible available targets, thus it must be $v \leq \rho$ at all time, too.

By the first equation in (1), we have that free cadherins diffuse and may change their status, becoming fixed, following the reaction term $-r(u, v)$. Symmetrically, the second equation in (1) says that fixed cadherins may change their status becoming free following the reaction term $r(u, v)$. Hence, $r(u, v)$ must describe the gain, $r_+(u, v)$, and loss, $r_-(u, v)$, rates of fixed particles.

The gain rate r_+ must be proportional to : the density u, i.e. the more free cadherins are present at a given place, the more of them are susceptible to adhere on the substrate ; the density $\rho - v$, i.e. the density of free targets available for fixation (this term ensures that v remains bounded by ρ) ; the aggregation function $F(v)$. We recall that $F(v)$ must be an increasing, positive and bounded function of v, and note that it must depend on the adhesion rate for cadherins, representing the probability of a free cadherin to link to the substrate without any other biological factor, augmented by the fact that locally other cadherins are fixed, that is the larger v is, the larger should be the value of $F(v)$, and the closer to 0 v is, the smaller $F(v)$ should be.

Analogously the unbinding rate r_- must be proportional to : the density of fixed cadherins v; the unbinding function $G(v)$. We recall that the function G is decreasing, positive and bounded with respect to v. That is the smaller is v, the larger is the value of $G(v)$, and the more v is close to ρ the smaller is $G(v)$. Note that the density of free cadherins u doesn't play any role in the unbinding rate r_-.

By the previous considerations we can define $F(v)$ and $G(v)$ as follows,

$$F(v) = \frac{a + \tanh(v)}{a + \tanh(\rho)} \, , \quad G(v) = 1 - \tanh(\alpha v), \tag{2}$$

where $a > 0$ is the adhesion rate and the sigmoid $\tanh(v)$ represents the aggregation effect we have previously described. In the definition of the function

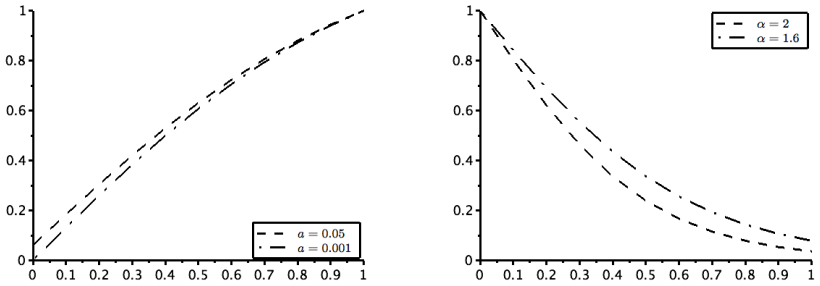

Fig. 2 Examples of F and G.

$G(v)$, the parameter α permits to concentrate or expand the effect of the unbinding : the larger α is, the stiffer the slope of the sigmoid $G(v)$ will be and the narrower will be the effect of the unbinding. A graphic representation of these functions is given in Fig. 2.

The choice to define the aggregation function only on the v variable is not anodyne. In fact, we can relate this dependence to the distance of the cell membrane to the substrate (or membrane fluctuation) : the more the membrane is distant, the less free cadherins are influenced by the presence of the fixed one, thus the value of the aggregation function should be smaller. Finally, we prove in the following proposition that assuming that the density v is positive and bounded, then both the aggregation function and the unbinding one are bounded, too.

Proposition 1 *If $v \in [0, \rho]$ then $F(v)$ and $G(v)$ belong to $[0, 1]$.*

Proof. Note that $F(v)$ is a continuous and strictly increasing function on the bounded domain $[0, \rho]$. Hence its minimum is taken at $v = 0$, that is $F(0) = a/(a + \tanh(\rho)) > 0$, and its maximum is taken at $v = \rho$, that is $F(\rho) = 1$. Hence, $0 < F(v) \leq 1$ for all $v \in [0, \rho]$.
Concerning $G(v)$, it is a continuous and strictly decreasing function on the bounded domain $[0, \rho]$. Hence its minimum is taken in $v = \rho$, that is $G(\rho) = 1 - \tanh(\alpha\rho) > 0$, and its maximum is taken in $v = 0$, that is $G(0) = 1$. Hence, $0 < G(v) \leq 1$ for all $v \in [0, \rho]$. □

We finally conclude the description of our model defining the reaction term $r(u, v)$ as follows,

$$r(u, v) = r_+(u, v) - r_-(v) = u(\rho - v)F(v) - vG(v), \tag{3}$$

and endowing the system (1) by suitable smooth initial conditions :

$$0 \leq u_0(x) \quad \text{and} \quad 0 \leq v_0(x) \leq \rho \tag{4}$$

as well as a Neumann homogeneous boundary conditions :

$$\nabla u \cdot \nu = 0 \quad \text{on} \quad \partial\Omega \tag{5}$$

where ν is the exterior unit vector normal to $\partial\Omega$. Note that there is no need to define a boundary condition for v. These boundary conditions ensure that no mass u is lost from the boundary.

Since the global population of cadherins on the membrane is made of free and fixed ones, we can consider that we have a total density distribution of cadherins given by $u+v$, which mass should be conserved when both u and v evolve. We normalize the initial data (u_0, v_0) so that:

$$\int_\Omega u_0(x) + v_0(x)\ dx = 1. \tag{6}$$

Thanks to (5), it is easily seen that the total mass is conserved. Infact, summing the equations in (1) and integrating over Ω, we have:

$$\partial_t \int_\Omega u + v\ dx = 0,$$

and thus, for all time $t \geq 0$,

$$\int_\Omega u(x,t) + v(x,t)\ dx = \int_\Omega u_0(x) + v_0(x)\ dx = 1.$$

3 Analytical results

Now that all the elements of the model are posed, in this section, we consider some more theoretical aspects. It is clearly important to prove that the system (1) admits positive and bounded solutions from a biological point of view, otherwise the model is nonsense. Nevertheless, these aspects are beyond the scope of this paper and will be addressed in a more general framework in future works.

We deal here with the stability of the stationary solutions of the associated problem. Indeed, stable steady states are interesting from a biological point of view, because they characterize the behavior of the studied system at equilibrium, so that the solution of the system should converge for large times to the steady state. As it is known, when considering reaction-diffusion systems in which the ratio of the diffusion coefficients is very small (one of the population diffuses much more slower than the other one), it is possible to obtain stationary solution which aren't homogeneous in space and which form structures, see [8] for an overview of this kind of models appearing in biology. We note that we are considering an extreme case with respect of those considered in [8], since one of the diffusion coefficient is zero, and we then have a degenerate

reaction-diffusion system.

We first consider the solutions to the stationary problem associated to (1), and then pass to the analysis of the steady states of (1), and of their instability, proving the creation of spatial patterns for some choices of the parameter a and α. The stationary problem associated to (1), reads:

$$\begin{cases} \Delta u = 0 \\ r(u,v) = 0 \end{cases} \tag{7}$$

completed with Neumann boundary conditions (5) on $\partial\Omega$. We assume for simplicity that Ω is normalized to 1, $|\Omega| = 1$.

Concerning the existence of a stationary solution to (7), we have the following result.

Proposition 2 *Under the hypothesis (6), there exists at least one homogeneous solution (U,V) to (7) endowed by (5). Moreover, this stationary solution (U,V) belongs to the interval $]0,1[\times]0,\rho[$.*

Proof. It is easily seen that the only solution $u(x)$ satisfying both the Neumann boundary condition and the first equation in (7) must be constant in x, $u(x) = U$ for all $x \in \Omega$. Hence, replacing $u(x) = U$ in (3), it is clear that, if it exists, the function $v(x)$ such that $r(U, v(x)) = 0$ must be constant too, $v(x) = V$ for all $x \in \Omega$. Thus, if it exists, the solution (U,V) to (7) is homogeneous in space.
Considering now hypothesis (6), and that $|\Omega| = 1$, we obtain that $U = 1 - V$. Therefore, the resolution of (7) is reduced to find a $V \in [0,\rho]$ such that:

$$(\rho - V)(1 - V)F(V) - VG(V) = 0.$$

Let us define the function $f : \mathbb{R} \to \mathbb{R}$ as:

$$f(v) = (\rho - v)(1 - v)\frac{a + \tanh(v)}{a + \tanh(\rho)} - v(1 - \tanh(\alpha v)),$$

and note that $f(0) = a\rho/(a+\tanh(\rho)) > 0$ and that $f(1) = -(1-\tanh(\alpha)) < 0$. Moreover, since f is a continuous function on $\mathbb{R}$, then there exists at least one $V \in]0,1[$ such that $f(V) = 0$. Finally, since $V \in]0,1[$, then $U = 1 - V \in]0,1[$, too.
Thus, to conclude the proof we must prove that V is always smaller than ρ. If $\rho > 1$, since $]0,1[\subset]0,\rho[$, then $V \in]0,\rho[$.
Otherwise, if $\rho \leq 1$, since $f(\rho) = -\rho(1 - \tanh(\alpha\rho)) < 0$, by the same arguments as before we can conclude that there exists at list one $V \in]0,\rho[$ solving $f(v) = 0$. This, concluding the proof. □

Due to the non linearity of $F(v)$ and $G(v)$, the value V cannot be given analytically, but we can compute it numerically for each suitable choice of parameters a and α. Let us note that, for large values of α, it become difficult to compute numerically the value of V because there are two values v both close to 1 satisfying $f(v) = 0$ and that for small values of a, the function $f(v)$ has almost a flat profile in $v = 1$.

Once proved the existence of the homogeneous stationary solution (U, V) we can study its stability. We have the following result.

Proposition 3 *Under the hypothesis (6), if*

$$\left[\ln\left(\frac{F}{G}\right)'\right]_V - \frac{\rho}{V(\rho - V)} \leq 0. \tag{8}$$

holds, then the homogeneous stationary solution (U, V) is stable.
Otherwise, (U, V) is unstable, and patterns formation occurs.

Proof. In order to study the stability of (U, V) we first have to linearize system (1). Let us note that U and V are linked by the following relation:

$$U = \frac{VG_V}{(\rho - V)F_V}, \tag{9}$$

with $F_V = F(V)$ and $G_V = G(V)$.
Moreover, let us define $A = \partial_u r|_{(U,V)}$ and $B = \partial_v r|_{(U,V)}$. Then a simple computation gives:

$$A = (\rho - V)F_V \ , \quad B = \frac{V(\rho - V)(G_V F'_V - F_V G'_V) - \rho F_V G_V}{(\rho - V)F_V}, \tag{10}$$

where

$$F'_V = \frac{dF}{dv}(V) = \frac{1 - (\tanh(V))^2}{a + \tanh(\rho)}$$

and

$$G'_V = \frac{dG}{dv}(V) = -\alpha(1 - \tanh(\alpha V)^2).$$

Then the linearized system reads:

$$\begin{cases} \partial_t u = \sigma \Delta u - A\ u - B\ v \\ \partial_t v = A\ u + B\ v \end{cases} \tag{11}$$

Let us now seek for a solution with u and v respectively given by:

$$u = e^{\lambda t}\hat{u} \ , \quad v = e^{\lambda t}\hat{v}, \tag{12}$$

where $\hat{u} = \hat{u}(k)$ and $\hat{v} = \hat{v}(k)$ are the respective Fourier transforms. Replacing (12) in (11) and dividing by $e^{\lambda t}$, we obtain the following linear system:

$$\begin{cases} \lambda u + \sigma\ k^2\ u + A\ u + B\ v = 0 \\ \lambda v - A\ u - B\ v = 0 \end{cases} \tag{13}$$

Clearly, $u = v = 0$ is a solution to (13), but we seek for non trivial solution to system (13). Hence the determinant of the associated matrix:

$$M = \begin{pmatrix} \lambda + \sigma\ k^2 + A & B \\ -A & \lambda - B \end{pmatrix},$$

must be zero. This leads to the following definition of the eigenvalues:

$$\lambda = \frac{-(\sigma\ k^2 + A - B) \pm \sqrt{(\sigma\ k^2 + A - B)^2 + 4\ \sigma\ k^2 B}}{2}, \tag{14}$$

which sign depends on the sign of A and B.
Note that, in order to have stable solutions, the eigenvalues λ must be negative, so that as time goes to ∞ the solution (u, v) converges to the stationary value (U, V), see [8] for more details. It is easily seen that $A > 0$ and that the sign of B depends on the sign of the numerator in (10).
If $B < 0$, then $(\sigma\ k^2 + A - B) > 0$ and $4\ \sigma\ k^2 B < 0$, so that the numerator in (14) is always negative, and both eigenvalues are negative too. In this case the stationary solution (U, V) is stable, and no pattern formation is possible.
If $B = 0$ then the eigenvalues are given by 0 and $-2(A+\sigma\ k^2)$ which is negative for all k. Thus, in this case, the stationary solution (U, V) is also stable.
Otherwise, if $B > 0$ then we have two possibilities. Or $0 < B < A + \sigma\ k^2$, or $0 < A + \sigma\ k^2 < B$. It is easily seen that both cases lead to the same result, that is, one negative and one positive eigenvalues. So that pattern formation may occur.
To conclude the proof, we finally have to show that $B \leq 0$ if and only if (8) holds. From (10) we get that $B \leq 0$ if and only if

$$V(\rho - V)(G_V F'_V - F_V G'_V) \leq \rho F_V G_V,$$

that is, since V, $\rho - V$, $F(v)$ and $G(v)$ are positive:

$$\frac{G_V F'_V - F_V G'_V}{F_V G_V} \leq \frac{\rho}{V(\rho - V)}.$$

It is now easy to see that the left hand-side in the previous inequality is equal to the first term in (8), concluding the proof. □

Due to the complexity of relation (8), it is not possible to give analytical conditions on the parameters a and α such that (8) holds or not. We thus use numerics and show in Fig. 3 that the sign of B may be negative for a large range of a and α (the black region). In particular, when $\alpha = 1$, suggesting that binding and unbinding forces may not by symmetric in v if we want pattern formation to occur. On the contrary, the sign of B is positive for a and α in a small domain, the white region. For parameters a and α in this region, the stationary state (U, V) is thus unstable and patterns formation occurs (see Fig. 7 and 4). In order to show the patterns formation in numerical simulations, we thus choose the parameters a and α in the white domain.

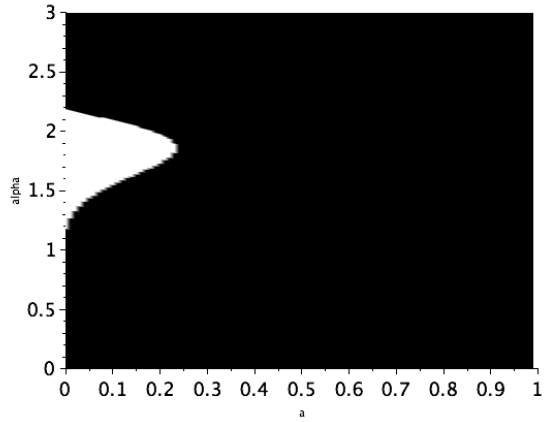

Fig. 3 The sign of B in the parameters domain $(a, \alpha) =]0, 1] \times [0, 3]$. Black region corresponds to $B \leq 0$ (stable solution (U, V)). White region corresponds to couples of parameters a, α for which $B > 0$ (unstable solution (U, V)).

4 Numerical results

In this section we first present some numerical tests showing the patterns formation for some theoretical data. Then we take into account the biological aspect of our problem and show on numerical results the different behaviors of the solutions in the biological framework.

We apply a finite differences discretization of system (1). As it is rather classic we just resume briefly our scheme. We define the space step Δx and Δy, and the grid points $x_i = i\Delta x$ and $x_j = j\Delta x$ for $i, j = 0, 1, 2, \ldots N$, where N is the number of discretization points. Let t^n be the discretized time defined by $t^n = n\Delta t$, where the time step Δt must satisfy a stability condition which is given by the discretization of the diffusion term (see (15)). Define $u^n_{i,j} = u(t^n, x_i, x_j)$ and $v^n_{ij} = v(t^n, x_i, x_j)$ the approximations of the density functions u and v, and $r^n_{ij} = r(u^n_{ij}, v^n_{ij})$ the discretization of the reaction term $r(u, v)$. Then the numerical scheme solving (1) is given by:

0. Determine V and if it does yield to instabilities
1. Determine the time step by

$$\Delta t = 0.1 \min\left(\frac{\Delta x^2}{4\sigma}, \frac{\Delta y^2}{4\sigma}\right) \tag{15}$$

2. Initialize v^0_{ij} and $u^0_{ij} = 1 - v^0_{ij}$, then at each time iteration
3. Compute $r^n_{ij} = u^n_{ij}(\rho - v^n_{ij})F(v^n_{ij}) - v^n_{ij}G(v^n_{ij})$

4. Compute u_{ij}^{n+1} and v_{ij}^{n+1} by :

$$u_{ij}^{n+1} = u_{ij}^{n} - \sigma \Delta t (Du)_{ij}^{n} - \Delta t \ \varepsilon r_{ij}^{n}$$
$$v_{ij}^{n+1} = v_{ij}^{n} + \Delta t \ \varepsilon r_{ij}^{n}$$

where $(Du)_{ij}^{n}$ is a classical centered discretization of the second derivatives.
4. Check the stop criteria

Note that the solution u of system (1) will always converge to a homogeneous solution in x, because of the diffusion term, the interesting result is the v distribution. Hence, in the following figures we show the density v for a time large enough so that equilibrium have been reached.

Another interesting data we can compute is the time evolution of the proportion of fixed cadherins $N_v(t)$, and the one for free cadherins, $N_u(t)$. In the sequel we shall call N_v the Immobile Fraction, and N_u the Mobile Fraction, in agreement with the experimental data showed in Table 1. These two quantities correspond to the zeroth order moments of the solutions $v(t)$ and $u(t)$:

$$N_v(t) = \int_\Omega v(t)dx \ , \quad N_u(t) = \int_\Omega u(t)dx. \tag{16}$$

Note also that since we have the total mass conservation, see (6), then the evolution of $N_u(t)$ is determined by $1 - N_v(t)$.

These quantities are of interest from a biological and chemical point of view because we know that they must both converge to a constant value (saturation process). In Table 1 we resume some of the corresponding values observed in experiments. Moreover, this convergence is assumed to be exponential and to behave like $S - e^{-kt}$, where S is the limit saturation value. Then, imposing that $N_v(t) = S - e^{-kt}$, we have that k can be numerically evaluated by means of a linear regression on the function $-\ln(S - N_v(t))$. As it will be shown in Fig. 10, the frequency ε plays a central role in order to fit our numerical exponential coefficient k to those obtained in experiments. Moreover, the convergence of $N_v(t)$ towards the saturation value S is actually exponential on the first portion of time and slow down when N_v get close to the limit value S.

4.1 Patterns formation

Recalling that structures forms when perturbing the homogeneous stationary solution (U, V), the initial data, in the first two testes, are defined by small perturbations of (U, V). We define either a random perturbation at each point $x \in \Omega$, see Fig. 4, or a perturbation given only in the center x_c of the domain Ω, see Fig. 7. These are not biological relevant tests, but we use them to present and discuss the possible behaviors of the solutions with respect to the choice of the parameters a and α. We have fixed the domain Ω to be the square

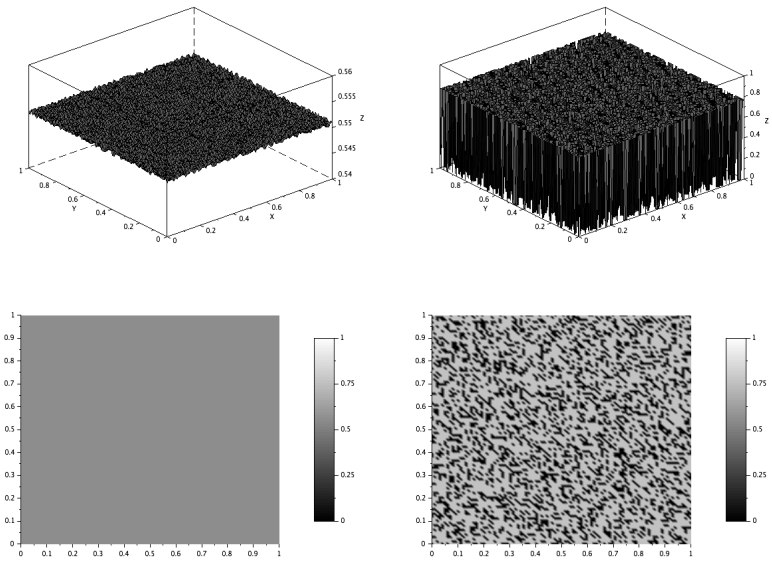

Fig. 4 Initial data, random uniform perturbation of (U, V). Final time $T = 500$, $a_0 = 0.005$, $\alpha = 1.8$, $\rho = 1$, $\sigma = 0.005$ and $\varepsilon = 1$. Top left: 3D plot of the initial data v_0. Top right: 3D density distribution v. Bottom left: 2D representation of the initial data v_0. Bottom right: 2D representation of the v distribution at final time T.

$[0, 1] \times [0, 1]$ and we choose $N = 100$ discretization points on each direction.

In Fig. 4, the perturbation is randomly given on the whole domain Ω. The initial data then reads:

$$v_0(x) = V + R_1(x), \tag{17}$$

where the perturbation amplitude is represented by $R_1(x)$ which is a random value of order 10^{-3}, which is too small to be detected in the 2D representation of the initial data v_0 (bottom left). The formation of structures where the particles have aggregated and are fixed to the substrate is clearly shown in both the 2D (bottom right) and 3D (top right) plots. Note that at equilibrium the aggregated domain (the set of the light-gray regions in the 2D plot) have all the same maximum value $\max(v)$ around 0.7, and that the transition to the unbound domain (dark region in the 2D plot) is very sharp.

In Fig. 5 we show the time evolution of $N_u(t)$ (dashed line) and $N_v(t)$ (dot-dashed line) starting from the initial data (17). After a transition period corresponding to the period during which both functions u and v slowly diverges from the stationary values U and V, a sharp transition takes place at a critical time t_c (which value is close to 90 for this run) after which each moment stabilizes to a new value. The critical time t_c represents the moment

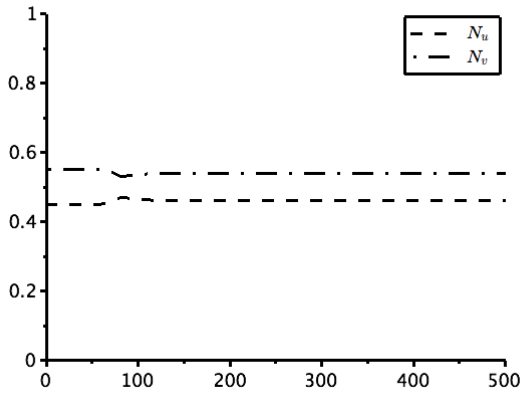

Fig. 5 The time evolution of $N_u(t)$ (dashed line) and $N_v(t)$ (dot-dashed line) starting from a random perturbation of the stationary solution (U, V).

at which the structures become spatially delimited by the important growth of the density of fixed cadherins thereby contained. Note that this example is not biologically relevant, since the percentage of fixed cadherins at initial time is already higher than the one for free cadherins, but it numerically shows that stationary solution are not stable for a and α opportunely chosen.

Next we consider a initial condition $v_0 = v(x, 0)$ defined by a small gaussian perturbation in the center of the domain Ω, see Fig. 6:

$$v_0 = V + 0.001 \exp\left(\frac{-(x - x_c)^2}{0.0001}\right),$$

with V the stationary value and x_c the center of the computational domain, $x_c = (0.5, 0.5)$.

We show in Fig. 7, the distributions of v when the equilibrium is reached. Note the formation of circular structures where the particles are aggregated. We did expect the central adhesion region, corresponding to where the gaussian is defined, but other adhesion regions are created around it. This may be caused by the fact that the cadherin aggregation around the gaussian center x_c leads to a variation of the densities u and v in the neighborhood of the gaussian, yielding a new perturbation of the stationary value V and thus to the formation of new aggregation junctions. This was not the case in the previous test, because the stationary value V was perturbed everywhere in the domain Ω and not enough space was left to other adhesions regions to appear. Again, as expected, a small perturbation of the stationary state, leads

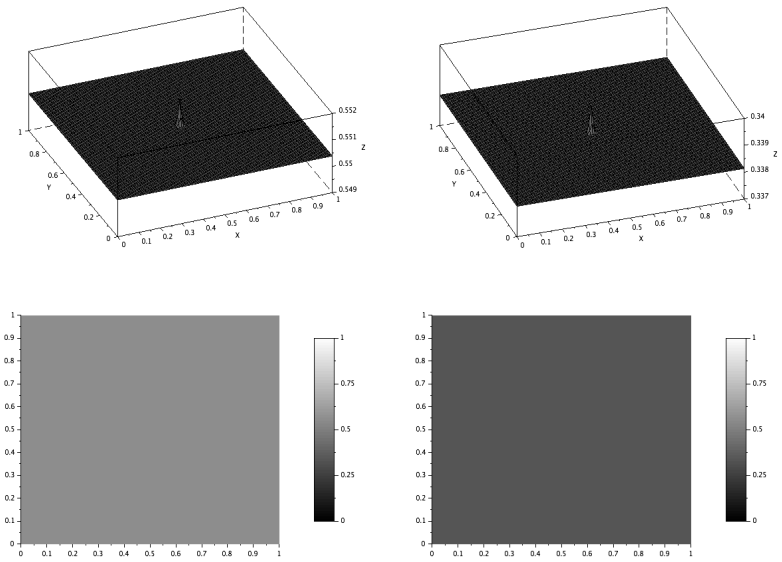

Fig. 6 Initial data v_0 given by a small gaussian perturbation of the stationary value V. Left : v_0 for parameters $a = 0.005$, $\alpha = 1.8$. Right : v_0 for parameters $a = 0.005$, $\alpha = 1.4$. Both initial data v_0 are plotted in 3D (top) end 2D (bottom).

to the formation of structures.

4.2 Biological framework

We now consider some more biological relevant frameworks and tests. Since our model is defined at a macroscopic scale, it is non-sense to describe the evolution of the densities at the cadherin scale, and thus we assume the domain Ω to be a square of length equal to 10 μm, with $N_x = N_y = 100$ grid points, that is a mesh size $\Delta x = \Delta_y = 0.1$ μm. We fix the target density value $\rho = 1$, and, accordingly to [5], we take the diffusion coefficient $\sigma = 3.3 \cdot 10^{-2} \mu m^2/s$. The frequency ε is first fixed to 1 s^{-1}, and in a last test it will be fitted so to obtain a good agreement for the exponential coefficient k.

Concerning the initial condition v_0, we recall that it heavily influence the final distribution v. Since no data is given by experiments, we assume that initially there are no fixed cadherins, so that $v(0, x)$ must be close to zero for all $x \in \Omega$. Moreover, we take into account the fact that the membrane may not have a flat profile by defining the initial data v_0 by the sum of N_g gaussians randomly distributed on the domain. The choice of each gaussian center is done in such a way that gaussians are sufficiently separated, so that

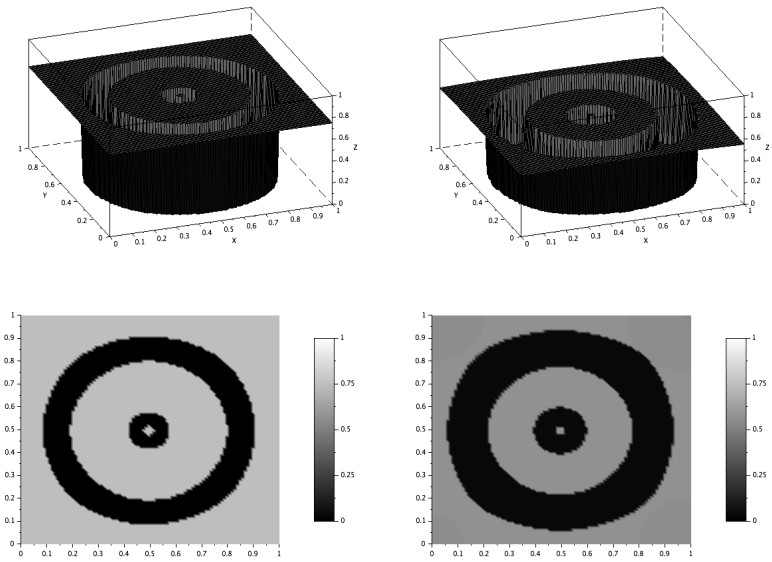

Fig. 7 Density v distributions at equilibrium (final time $T = 500$). Left: the solution for the parameters $a = 0.005$, $\alpha = 1.8$, $\rho = 1$ and $\sigma = 0.005$. Right: the solution for the parameters $a = 0.005$, $\alpha = 1.4$, $\rho = 1$, $\sigma = 0.005$ and $\varepsilon = 1$. For both tests we traced the the 3D plot (top) and the 2D representation (bottom).

each gaussian may be also seen as a single beginning of aggregate, but these centers are not too far, so that aggregates may also interact. The gaussians eight is also randomly defined while their standard variation is fixed in such a way that each gaussian support covers more than one mesh, and eventually has a small overlap with neighboring gaussians. The initial data v_0 then reads:

$$v_0(x) = \sum_{k=1}^{N_g} R_k \exp\left(\frac{(x - x_k)^2}{0.0225}\right), \tag{18}$$

where R_k is a random value between 0 and 0.005, and the centers x_k are such that the distance $\|x_k - x_i\|$ between x_k and all others centers x_i, with $i \neq k$ is larger than 0.5. The number of gaussian N_g has to be fixed, and we choose it large enough so that it is almost not possible to have N_g+1 gaussians satisfying the previous requirements ($N_g = 266$ in our computations). We show in Fig. 8 the 2D representation of the initial gaussian distribution we choose. Note that the scale of the plot is between 0 and the maximum value of v_0, that is 0.005.

Since computational times may be long, we define a stop criteria by a control on the evolution of the discrete zero moment for the fixed cadherin population, N_v. Each *niter* iterations we compute the Immobile Fraction $N_v(t^{niter})$ and we compare it to the previous one. When the absolute error between this

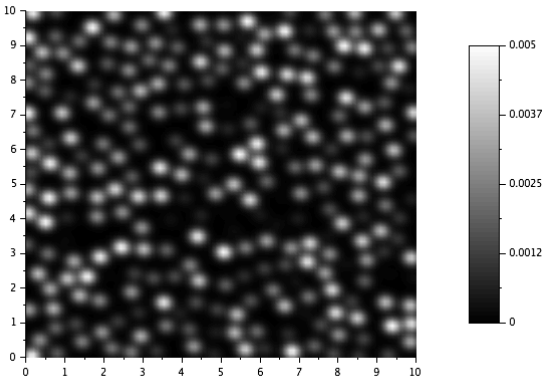

Fig. 8 The initial data v_0 defined by (18).

two quantities is close to zero (e.g., smaller than a given precision 10^{-6}), then we stop our computation. Some of the numerical results obtained are given in the following figures.

In Fig. 9 we show the final density v distribution (left) and the time evolution for the Immobile and Mobile Fractions N_u and N_v (right), for various couples of parameters a and α, for $\varepsilon = 1$. Computations are always stopped when the stop criteria is reached. In A) we choose a small adhesion rate $a = 0.001$ and a large value of the slope $\alpha = 2$, the result being a set of interconnected circular regions of adhesion with a maximum value of v around 0.8 and a minimum at almost zero. The Immobile Fraction N_v has grown form 0 to almost 0.6 (dot-dashed line), while the Mobile Fraction N_u has decreased to almost 0.4 (dashed line). When increasing the adhesion rate to $a = 0.05$, keeping $\alpha = 2$, see B), then the adhesion regions almost cover the whole domain, yielding to a smaller maximum for v and a larger minimum, but still in a range of values implying that almost all cadherins have bound in the adhesion region and almost only free cadherins exist elsewhere. Again, we end up with more fixed cadherins than free one, but the convergence to the saturation value S is much faster, the N_v slope is sharper than for A). This may be induced from both the adhesion and aggregation effects. The Immobile Fraction N_v has grown form 0 to more than 0.6 (dot-dashed line), while the Mobile Fraction N_u has decreased to less than 0.4 (dashed line). The same behavior can be observed between C) and D). Note that in this two cases is D) which has the smaller value for a, and the main difference with A) and B) stands in the smaller slope value $\alpha = 1.6$. In both cases the Immobile Fraction N_v tends to stabilize around smaller values, 0.5 for C) and 0.4 for B). Finally times needed to reach the saturation value S are smaller than for A) and B), while time to reach the equilibrium (stop criteria) are slightly larger for C) and D), than for A) and

B).
When comparing A) with D) and B) with C), that is when fixing the adhesion rates a and changing the slopes α, we note that the maximum value for v is smaller in D) and C) than in A) and B), and also that the minima is larger. Thus, the influence of the slope α in the unbinding function, is translated in the obtention of more interconnected adhesion regions for large α as well as higher values for v. Concerning the evolution of N_v and N_u, the convergence seems to behave similarly for A) and D), and for B) and C).

We finally note that, although close saturation levels are obtained for the parameters of test A), B) and C), D), the values of the maximum and minimum of the density v may significantly vary. In particular, for both C) and D) the maximum of v is between 0.5 and 0.7, and more in C) the minimum is slightly larger than 0 so that we can't conclude that in the non-adhesion region (dark one) there are no fixed particles. Even thought, we don't have clear biological insight of the real value of the density in the junction area, we argue that, at equilibrium, in the junction regions, the density may be close to ρ. Therefore, parameters for which the maximum and minimum of v are between 0.1 and 0.7, may not be admissible from a biological point of view. Thus, in the sequel we'll choose the parameters in such a way that we approach the saturation level and that the maximum and minimum for v do not belong to the interval $]0.1, 0.7[$.

All these examples show a saturation of the both the values $N_v(t)$ and $N_u(t)$ as times is large enough. This fact has been also highlighted in several experiments. We resume in Table 1 the values for the Immobile Fraction which was observed. Note that these values range in the interval 0.3 to 0.7, which correspond also to what we observe numerically for the $N_v(t)$ values. Moreover, the Mobile Fraction in experiments turns to be equal to 1 minus the Immobile Fraction value, and this is the same in our model, since, as already underlined, $N_u(t) = 1 - N_v(t)$.

Table 1 Experimental saturation values for the Immobile Fraction, corresponding to $N(v)$ at equilibrium.

Cadherin type	Cell Type	**Immobile Fraction**	Mobile Fraction	Reference
E-cadherin	MDCK	**0.6-0.7**	0.3-0.4	[12]
N-cadherin	C2C12	**0.6**	0.4	[6]
N-cadherin	neurons	**0.3**	0.7	[10]
E-cadherin	A431	**0.3-0.4**	0.6-0.7	[9]
E-cadherin	MDCK	**0.5-0.6**	0.5-0.6	unpublished
N-cadherin	HEK	**0.4-0.6**	0.4-0.6	unpublished

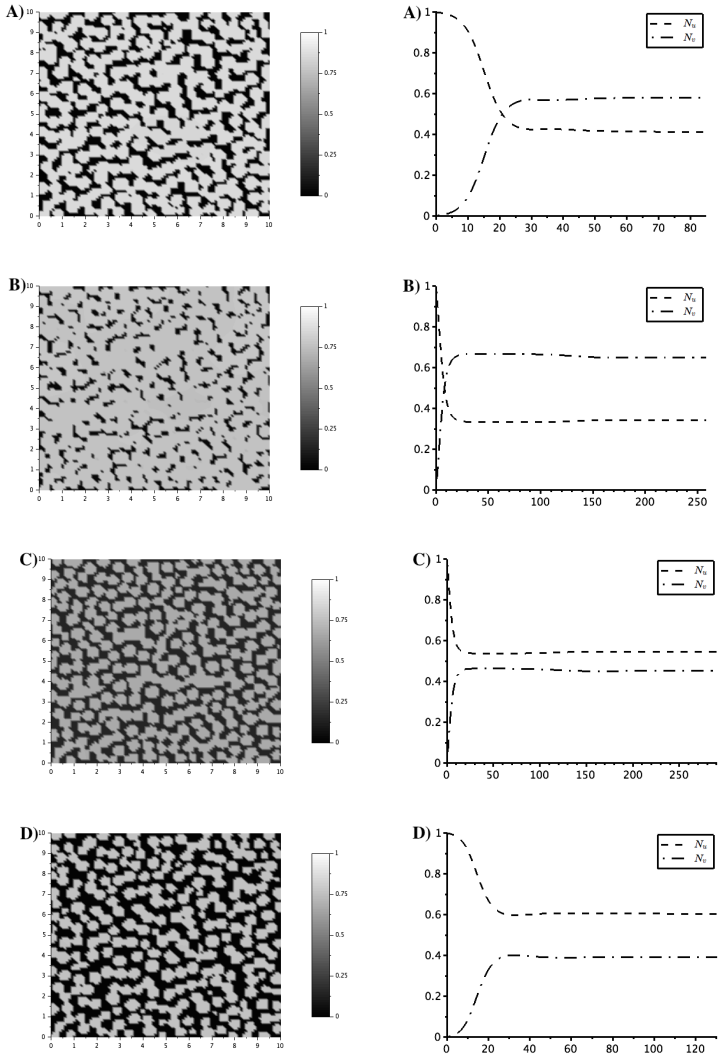

Fig. 9 The final 2D representation density v (left) and the time evolution for N_u and N_v. The parameters are $\rho = 1$, $\sigma = 3.3 \cdot 10^{-2}$, $\tau = 1$ and for figures: A) $a = 0.001$, $\alpha = 2$; B) $a = 0.05$, $\alpha = 2$; C) $a = 0.05$, $\alpha = 1.6$; D) $a = 0.001$, $\alpha = 1.6$.

We consider now the experiments form [10], for which we now that the saturation value of the Immobile Fraction N_v is almost 0.35, and that the convergence has an estimated exponential coefficient $K = 13\ h^{-1} = 3.61 \cdot 10^{-3}\ s^{-1}$ (see the introduction of Sect. 4 for more details on the exponential behavior). We consider an initial data defined as in (18), but such that $N_v(0) \approx 0.1$, so that a first transitional period during which the first junctions appears re-

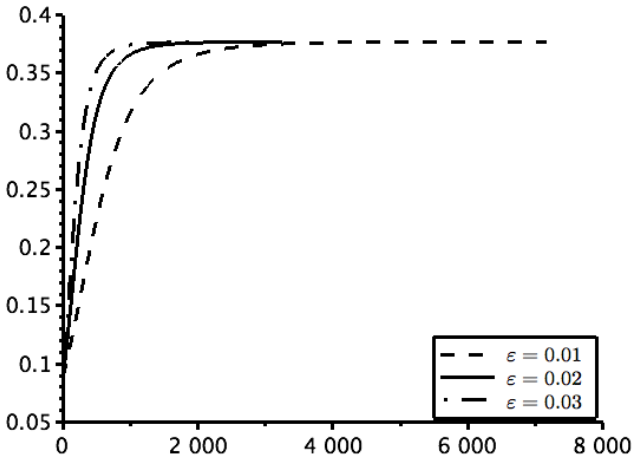

Fig. 10 Time evolutions of N_v for different values of the frequency : $\varepsilon = 0.01$ dot-dashed line, $\varepsilon = 0.02$ continuous line, $\varepsilon = 0.03$ dashed line. The parameters are $\rho = 1$, $\sigma = 3.3 \cdot 10^{-2}$, $a = 10^{-3}$, $\alpha = 1.65$.

duces to almost zero, but still the fixed cadherin density population N_v is much smaller than the free cadherins one N_u. Not considering this choice would just skip the exponential growth of $N_v(t)$ for larger times. Moreover, we fix the parameters as follows $a = 10^{-3}$ and $\alpha = 1.65$, $\rho = 1$, $\sigma = 3.3 \cdot 10^{-2}$, so that we obtain a saturation level S close to 3.7 and values for the maximum and minima of the density v respectively close to 1 and 0. The parameter playing a central role here is the frequency ε, which will vary in order to fit the exponential coefficient k to the experimental one K.

The results of our numerical simulations are shown in Fig. 10, where we plot the N_v time evolutions for three values of the frequency $\varepsilon = 0.01,\ 0.02,\ 0.03\ s^{-1}$. As shown the larger the frequency ε is, the sharper is the slope of the N_v curve, that is the smaller is the time needed to reach the saturation level as well as the equilibrium state.

Results for some more choices of the relaxation parameter ε, and for the same parameters as in Fig. 10 are given in the Table 2. The k coefficient are computed by means of a linear regression on the curve $-\ln(S - N_v(t))$, where S is the saturation limit and time t is restricted to a same initial time interval for all choice of ε. We can conclude that for a fixed set of parameters a, α, ρ and σ the choice of ε significantly influences the exponential rate of convergence, and that in our particular case the best choice is given by $\varepsilon = 0.02$ (note the really

Table 2 Relaxation parameters τ and corresponding exponential coefficients

ε	0.010	0.015	0.020	0.025	0.030
$k \cdot 10^{-3}$	1.6	2.7	3.6	4.5	5.1

good agreement of the computed k and the value obtained in experiments K).

5 Conclusion

We propose and study a phenomenological mathematical model intended to describe the cadherin aggregates formation at the cell-cell contact membrane in the absence of the actin cytoskeleton. This model is composed of two partial differential equation coupled by means of a reaction term which describes the way a cadherin may bind or unbind to one other, and which takes into account the effects of locally existing contacts. Each equation describes the time-space evolution of a cadherin population : the free ones, not linked to the substrate and diffusing, and the fixed ones, not diffusing. After having numerically proved that the model is able to reproduce the formation of aggregates, we construct a more biological framework and compare the results obtained by means of numerical simulations to experimental ones. In particular, the proposed model show a saturation of the density of both populations which is of the same order of the one observed in several experiments, see Table 1 and references therein. Further, suitably choosing the parameters of the model we are able to compute the supposed undergoing exponential convergence coefficient with a very good agreement with the one observed in [10].

This work is a first attempt to model the cell-cell junctions creation, and may be enriched and specified including more bio-physical aspects as modeling more precisely cis- or trans-contacts, or including the retrograde effect of the actin filaments, or considering a circular geometry included in the computational domain. Moreover, this work may have a much wider implication in biological processes since many adhesion receptors, channel proteins and other membrane-born proteins associate in clusters or oligomers at the cell surface. Their recruitment in discrete aggregates is often associated to their specific function and understanding the biochemical and physical principles that govern this process is of major importance.

Acknowledgements POS has been supported by an ANR funding (2010 Blan 1515). BS is supported by the Labex LMH (ANR-11-IDEX-003-02) and by the FMJH (ANR-Investissements d'Avenir). The authors thanks the CNRS, INRIA and INSERM for the founding of the PEPS-MBI project "MAC: Modélisation d'Adhésion des Cadhérines" the ANR 2010 Blan 1515 and Human Frontier Science Program grant RTG0040/2012, and the ANR blanche project "Kibord" (ANR-13-BS01-0004) funded by the French Ministry of Research.

References

1. Bihr, T., Seifert, U., Smith, A.S.: Nucleation of ligand-receptor domains in membrane adhesion. Phys. Rev. Lett. **109**, 258,101 (2012). DOI 10.1103/PhysRevLett.109.258101. URL http://link.aps.org/doi/10.1103/PhysRevLett.109.258101
2. Gavard, J., Lambert, M., Grosheva, I., Marthiens, V., Irinopoulou, T., Riou, J.F., Bershadsky, A., Mège, R.M.: Lamellipodium extension and cadherin adhesion: two cell responses to cadherin activation relying on distinct signalling pathways. Journal of Cell Science **117**(2), 257–270 (2004). DOI 10.1242/jcs.00857. URL http://jcs.biologists.org/content/117/2/257.abstract
3. Harrison, O.J., Jin, X., Hong, S., Bahna, F., Ahlsen, G., Brasch, J., Wu, Y., Vendome, J., Felsovalyi, K., Hampton, C.M., Troyanovsky, R.B., Ben-Shaul, A., Frank, J., Troyanovsky, S.M., Shapiro, L., Honig, B.: The extracellular architecture of adherens junctions revealed by crystal structures of type i cadherins. Structure **19**(2), 244 – 256 (2011). DOI http://dx.doi.org/10.1016/j.str.2010.11.016. URL http://www.sciencedirect.com/science/article/pii/S0969212611000037
4. Hong, S., Troyanovsky, R.B., Troyanovsky, S.M.: Binding to f-actin guides cadherin cluster assembly, stability, and movement. Journal of Cell Biology **201**(1), 131–143 (2013). DOI 10.1083/jcb.201211054. URL http://jcb.rupress.org/content/201/1/131.abstract
5. Lambert, M., Choquet, D., Mège, R.M.: Dynamics of ligand-induced, rac1-dependent anchoring of cadherins to the actin cytoskeleton. Journal of Cell Biology **157**(3), 469–479 (2002). DOI http://www.jcb.org/cgi/doi/10.1083/jcb.200107104
6. Lambert, M., Thoumine, O., Brevier, J., Choquet, D., Riveline, D., Mège, R.M.: Nucleation and growth of cadherin adhesions. Experimental cell research **313**(19), 4025–4040 (2007)
7. Mège, R.M., Gavard, J., Lambert, M.: Regulation of cell-ĂŞcell junctions by the cytoskeleton. Current Opinion in Cell Biology **18**(5), 541 – 548 (2006). DOI http://dx.doi.org/10.1016/j.ceb.2006.08.004. URL http://www.sciencedirect.com/science/article/pii/S0955067406001141
8. Murray, J.D.: Mathematical Biology II. Spatial Models and Biomedical Applications, vol. 18. Springer (2003). DOI 10.1007/b98869
9. Strale, P.O., Duchesne, L., Peyret, G., Montel, L., Nguyen, T., Png, E., Tampé, R., Troyanovsky, S., Hénon, S., Ladoux, B., Mège, R.M.: The formation of ordered nanoclusters controls cadherin anchoring to actin and cell-cell contact fluidity. Journal of Cell Biology **210**(2), 333–346 (2015)
10. Thoumine, O., Lambert, M., Mège, R.M., Choquet, D.: Regulation of n-cadherin dynamics at neuronal contacts by ligand binding and cytoskeletal coupling. Molecular Biology of the Cell **17**(2), 862–875 (2006). DOI http://www.jcb.org/cgi/doi/10.1091/mbc.E05-04-0335
11. Wu, Y., Honig, B., Ben-Shaul, A.: Theory and simulations of adhesion receptor dimerization on membrane surfaces. Biophysical Journal **104**(6), 1221 – 1229 (2013). DOI http://dx.doi.org/10.1016/j.bpj.2013.02.009. URL http://www.sciencedirect.com/science/article/pii/S000634951300194X
12. Yamada, S., Pokutta, S., Drees, F., Weis, W.I., Nelson, W.J.: Deconstructing the cadherin-catenin-actin complex. Cell **123**(5), 889 – 901 (2005). DOI http://dx.doi.org/10.1016/j.cell.2005.09.020. URL http://www.sciencedirect.com/science/article/pii/S0092867405009748